Influence of process parameters on the Aerosol Deposition (AD) of Yttriastabilized Zirconia particles

Tarini Prasad Mishra^{a*}, Reeti Singh^a, Robert Mücke^a, Jürgen Malzbender^b, Martin Bram^a,
Olivier Guillon^{a, c}, Robert Vaßen^a

^a Forschungszentrum Jülich GmbH, Institute of Energy and Climate Research IEK-1, 52428 Jülich, Germany

^b Forschungszentrum Jülich GmbH, Institute of Energy and Climate Research, IEK-2, 52428 Jülich, Germany

^c Jülich Aachen Research Alliance: JARA-Energy, Jülich 52425, Germany

Tel.: +49 2461 61-8058 *Fax*: +49 2461 61-5700

*Email address: t.mishra@fz-juelich.de (Tarini Prasad Mishra)

ABSTRACT

Aerosol Deposition (AD) is a novel deposition process for the fabrication of dense and rather thick oxide films at room temperature. The bonding of the deposited ceramic particles is based on a shock-loading consolidation, resulting from the impact of the ceramic particles on the substrate. However, the deposition mechanism is not fully understood. In addition, many technical challenges have been observed for achieving a successful deposition of the oxides with higher efficiency. In this work, the influence of different processing parameters on the properties of the deposited layer is studied. Proof of concept was done using 8 mol% Yttria Stabilized Zirconia (8YSZ) powder as starting material. The window of deposition with respect to carrier gas flows for successful deposition was identified. The influence of this carrier gas flow, the substrate materials and the carrier gas species on the coating thickness, interface quality and coating microstructure was systematically investigated. The derived mechanical characteristics revealed an unexpected behaviour related to a gradient microstructure. This study supports understanding of the mechanism of room temperature impact consolidation and its effect on the mechanical properties of the deposited layer.

Keywords: Aerosol Deposition Process; 8mol% Yttria stabilized zirconia (8YSZ) coating; Room temperature impact consolidation (RTIC); Carrier gas; Coating hardness

1- Introduction

Coating technologies are essential to provide surface protection, decorative finishes and numerous special applications (Ref 1). Many everyday products are only rendered usable because of their surface treatments. Ceramics coatings are used in particular to improve the resistance to sharp contact, wear and erosion (Ref 2). Also, they often improve the resistance to substrate oxidation because the coating separates the substrate from direct exposure to potentially harmful environmental conditions (Ref 3). Conventional fabrication of ceramics either by powder shaping and sintering or by coating processes requires high temperatures, usually above 1000°C (Ref 1,4). The high temperature necessary for a successful deposition of ceramics limits their integration with other materials like polymers and metals. Moreover, the high temperature deposition process for the ceramics is usually associated with high energy consumption.

Circumventing such problems, a novel deposition technique has been developed by Akedo et al. (Ref 5,6) that enables the formation of ceramic films at room temperature, which became known as Aerosol Deposition (AD) process. In this process, submicron sized particles are accelerated by a gas flow through a nozzle and ejected onto a substrate at a very low pressure. Upon impaction, the particle's kinetic energy is converted into an apparent bonding energy between substrate and between particles (Ref 6). The AD process is carried out entirely at room temperature under high vacuum, resulting in dense ceramic films (Ref 7). Since its invention many oxides were successfully deposited using the AD process, which has been summarized in a recent review paper (Ref 7). Due to the unique combination of processing parameters involved in the AD process ceramic films with new properties, which are difficult to achieve by traditional deposition methods, may result.

The suggested mechanism responsible for the successful deposition of ceramic particles onto a substrate during AD process considers the fragmentation and consolidation of the submicron particles (Ref 6,8). Upon collision of the submicron sized particles onto the substrate part of the kinetic energy is converted into bonding energy. As the process is carried out at room temperature, the mechanism is called "Room Temperature Impact Consolidation (RTIC)"(Ref 6,8,9). The dense structure of the AD coating is suggested to be a result of particle deformation upon impaction also attributed to a hammering effect (Ref 10). The fragmentation of the initial particles was verified by comparing the spectral peak broadening and slight shift in the peak position in X-Ray Diffraction (XRD) of deposited α -Al2O3 coating as compared to XRD of feedstock α -Al2O3 powder (Ref 6,9). Nevertheless, the exact mechanism responsible for the deposition of ceramics by the AD process is still under discussion (Ref 11).

Yittria Stabilized Zirconia (YSZ) due to its high melting temperature, high ionic conductivity, low thermal conductivity at higher temperatures and good mechanical properties at elevated temperatures finds many applications ranging from electrochemical devices (Ref 12), gas sensing devices (Ref 13) to thermal barrier coating in gas turbines (Ref 14). However, fabrication of YSZ materials typically requires very high temperatures. Focusing on the deposition methods, there are two primary techniques that might be used for the deposition of yttria stabilized zirconia, plasma spray (PS) and electron beam physical vapor deposition (EB-PVD) (Ref 15,16). Hence, deposition of dense and rather thick YSZ materials at room temperature by AD process is of high interest. However, until recently very few publication focused on the processing of YSZ materials by the AD process (Ref 17–19), where in fact especially the influence of the different processing parameters on the coating properties is still missing.

In the current work, 8 mol% Yttria Stabilized Zirconia (8YSZ) was successfully deposited by the AD process. The influence of different AD process parameters on the properties of the deposited layer was studied and the window of deposition with respect of carrier gas flows for successful deposition of 8YSZ powder by AD process was identified. The influence of carrier gas flow and stand-off distance (i.e. distance between nozzle and substrate) on the coating thickness, interface quality and coating microstructure was systematically investigated. Computational fluid dynamics (CFD) simulations was used to study the gas flow behaviour and estimation of the gas velocity. In terms of mechanical properties, the average hardness of the coatings is studied and its dependence on a variation of gas flows. In addition to that, the hardness of the coatings at different distances from the interface was assessed. Complementary microstructural studies aid the interpretation of the results.

2- Experimental

2.1- Starting Material

Commercially available 8 mol. % yttria stabilized zirconia powders (TZ-8Y, TOSOH Corporation, Tokyo, Japan) were used as the starting materials in the aerosol deposition process. The particle size distribution of the starting powder was measured with laser diffraction particle sizing LA-950 (2 laser diodes, HORIBA analyzers, Horiba Ltd., Kyoto, Japan). The morphology of the powder was observed by a scanning electron microscope (SEM, Zeiss Ultra 55 FEG-SEM, Carl Zeiss Microscopy GmbH, Oberkochen, Germany). Furthermore, the crystallite characteristics of the starting powder have been analyzed by performing X-ray Diffractometry (Bruker AXS GmbH, Karlsruhe, Germany) using Cu Kα radiation. Operating voltage and current were 40 kV and 40 mA, respectively. The lattice parameters were determined using Pawley's method, for the refinement the TOPAS software (Bruker Corporation, Germany) was utilized.

2.2- Substrate Preparation

Three different substrate materials were used in the current study, Pure Copper, 3 wt% Mg-Al alloy, stainless steel (Material No.-1.4571). The selection of the substrate materials were primarily based on the hardness values. From the manufacturers data sheet the Brinell hardness that were measured with a steel punch are HB 35, HB 63 and HB 215 for pure copper, 3 wt% Mg-Al alloy,

stainless steel (Material No.-1.4571) respectively. The substrates had dimensions of 24×24 mm². All substrates were prepared for the deposition process in two different conditions:

- I. polished with SiC grit paper, 4000 grades
- II. F-150; substrate grit blasted with Al₂O₃ particle with size in the range of 45 125 μm under an angle of approximately 90°, stand-off distance between 5-8 mm, using a pressure of 0.3 MPa and Argon as a carrier gas.

After grit blasting and polishing the substrates were cleaned with ethanol in an ultrasonic bath. Substrate thickness and weight were measured before the deposition.

2.3- Aerosol Deposition Process Set-up

The aerosol deposition process was realized by a custom-built apparatus developed inhouse. The principle of the process set-up is similar to the general AD process set-up reported in literatures (Ref 7,11,8). However, small modifications were made to the set-up to realize well dispersed particles for the AD process as shown in Fig. 1.

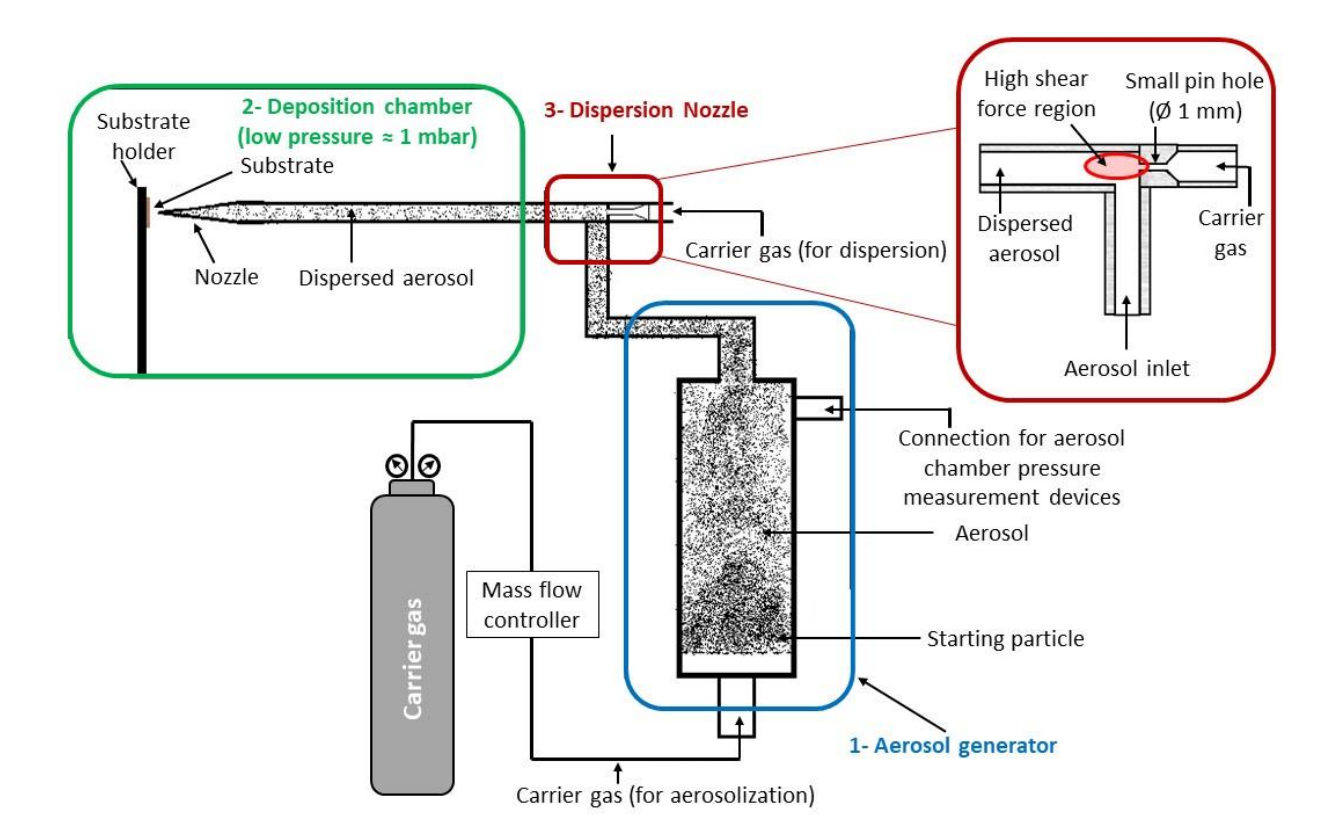


Fig. 1. Schematic illustration of the modified aerosol deposition process set-up used in this work, showing three key components: 1-Aerosol generator, 2- Deposition chamber and 3-Dispersion nozzle.

The aerosol generator had a metal filter of 4-micron pore size, which was placed at the bottom of the aerosol generator. The starting powder was placed inside the aerosol generator. The carrier gas was injected through the bottom of the chamber and the gas flow was controlled with a mass flow controller, to produce a fluidized bed. The aerosolized particles were then transported due to the pressure difference between aerosol generator and the deposition chamber. The aerosol generator was placed on a weighing machine to measure the mass difference before and after the deposition process. The aerosol generator was also connected with a valve to measure the aerosol chamber pressure during the deposition process.

All depositions were carried out in an Oerlikon Metco Multicoat facility for Very Low Pressure Plasma Spray (VLPPS) and Plasma Spray Physical Vapour Deposition (PS-PVD) (Ref 20). The minimum operation pressure of the facility was approximately 1 mbar. Inside the deposition chamber, the substrate was placed on a substrate holder which remained fixed during the deposition process. The nozzle was attached to the robotic arm which was able to move x-y-z directions and controlled electronically. The nozzle used in this work was a simple converging slit nozzle with a slit opening of 10 mm * 0.4 mm, as shown in Fig. 2.

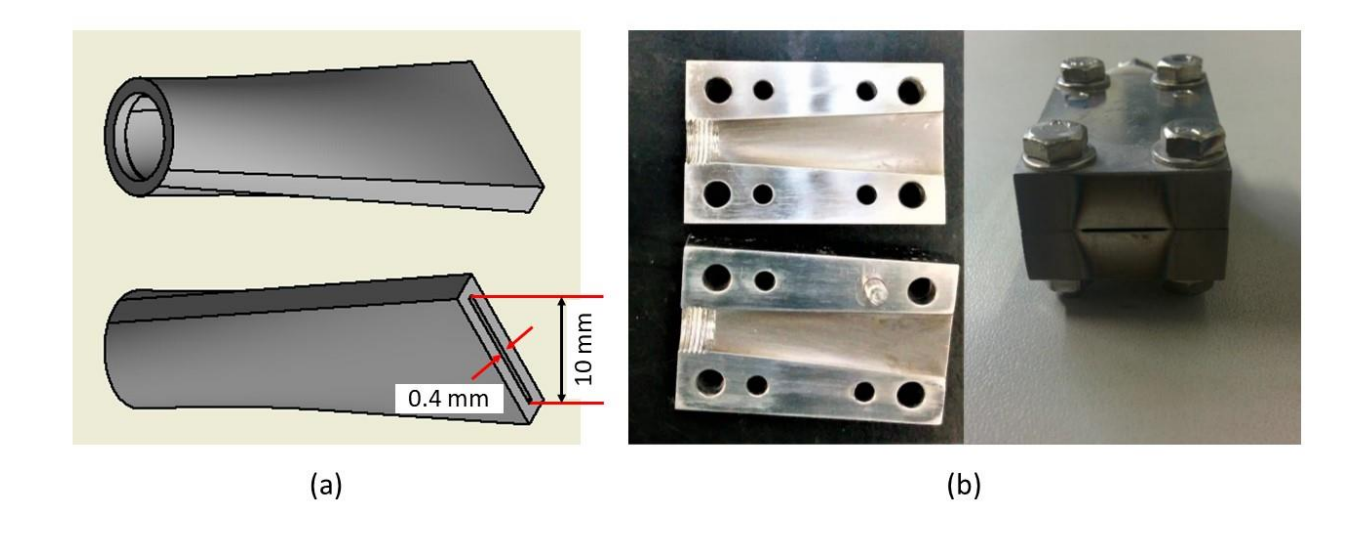


Fig. 2. (a) Sketch of the convergent slit nozzle and (b) image of the inside view and front view of the nozzle used in the current work.

A dispersion nozzle was incorporated between the aerosol generator and the deposition chamber to break the agglomerated particles. A constant gas flow of 5 SLPM (standard litre per minute) was used in the aerosol generator to generate the aerosol. The generated aerosol entered the dispersion nozzle through the bottom as shown in Fig. 1 (for aerosolization). The total carrier gas flow increased by an additional gas supply to the dispersion nozzle (for dispersion). This ensured a constant volume of powders transported to the deposition chamber for different carrier gas flows. In the dispersion nozzle, the additional gas flow was passed through a small pin hole (ϕ = 1 mm) to create a high shear force in front of it. The high shear force was able to break the agglomerated particles in the aerosol.

Surface topography and surface roughness of the coatings were measured with a double-sided optical profilometer (CyberScan CT 300, CyberTechnologies, Ingolstadt, Germany) using a chromatic white light sensor (CHR 3000, CyberTechnologies). The roughness value was calculated on a profile yielding the average roughness (R_a) was used.

The cross-sections of the samples were prepared by standard metallographic routes. Microstructure and the thickness of the deposited layers were analyzed from the SEM micrographs, which were obtained by using a Carl Zeiss Neon 40 Smart SEM V05.03 Field Emission Scanning Electron Microscope at a beam energy 25 keV, the working distance was approximately 7.5 mm and a BSE detector was used.

Quantitative analysis of the average volume fraction of the porosity was measured from the high-resolution SEM micrographs by digital image analysis (Image J) (Ref 21). Additionally, the cumulative percentage of the porosity and the pore size was measured by mercury intrusion porosimetry (MIP). The porosimeters used was PASCAL 440 up to a maximum pressure of 350 MPa (Porotec GmbH, Hofheim, Germany).

The average hardness of the deposited layer were measured by a CSM instruments (Anton Paar CSM Nano-Indentation Tester) equipped with a Berkovich tip for quantifying the localized hardness of the coatings. The maximum applied load was 10 mN with a linear loading and

unloading rate of 20 mN/min. At each coating, indentation was carried out at 4 different positions as a function of distance from the interface between the substrate and the coating. Additionally, at each position 5 indentation tests were performed and the average value was calculated. Hold period was 5 s, and acquisition rate was 10 Hz. The Oliver-Pharr theory was used as a physical principle and model to determine the hardness from the indentation load (*P*) versus displacement (*h*) data, which was obtained during one full cycle of loading and unloading cycle (Ref 22).

2.4- Flow field simulation

In this work, computational fluid dynamics (CFD) simulations were carried out with ANSYS Fluent 17.1 to study the gas flow behaviour and the gas velocity attains for the carrier gas flow rate of 10 slpm. The k- ω shear stress transitions (SST) model was used within a pressure based coupled solver to solve the Reynold averaged Navier Stokes equations including the temperature effect of viscous heating. The fluid properties of argon were taken as follows: density from the ideal gas equations allowing compression in supersonic flow, specific heat capacity $C_p = 520.64 \text{ J/(kg K)}$, thermal conductivity $k = [-3.81804 \times 10^{-8} \times (T/K)^2 + 7.280991 \times 10^{-8} \times T/K - 0.00060274] \text{ W/(m K)}$, viscosity $\eta = [-5.009371 \times 10^{-11} \times (T/K)^2 + 9.388371 \times 10^{-8} \times T/K - 9.123328] kg/(m s)$, molecular weight $\mu = 39.948 \text{ kg/kmol}$. The initial temperature of all gases was set to 300 K and the chamber pressure to 1.0 mbar. All walls were treated as no-slip walls.

3- Results and Discussion

3.1- Characterization of the starting powder

Figure 3 shows the SEM micrographs of the 8YSZ powder used for aerosol deposition process at two different magnifications revealing the as-received agglomerated state (Fig. 3 (a)) and the primary particles (Fig. 3 (b)). The as-received powder appears to be in a spray-dried, agglomerated state, however, when the starting powder was mixed with ethanol and dispersed by ultrasonic treatment the primary particles can be observed, which are of sub-micron sized. The measured particle size distribution confirmed the state of the particles as shown in the SEM micrographs.

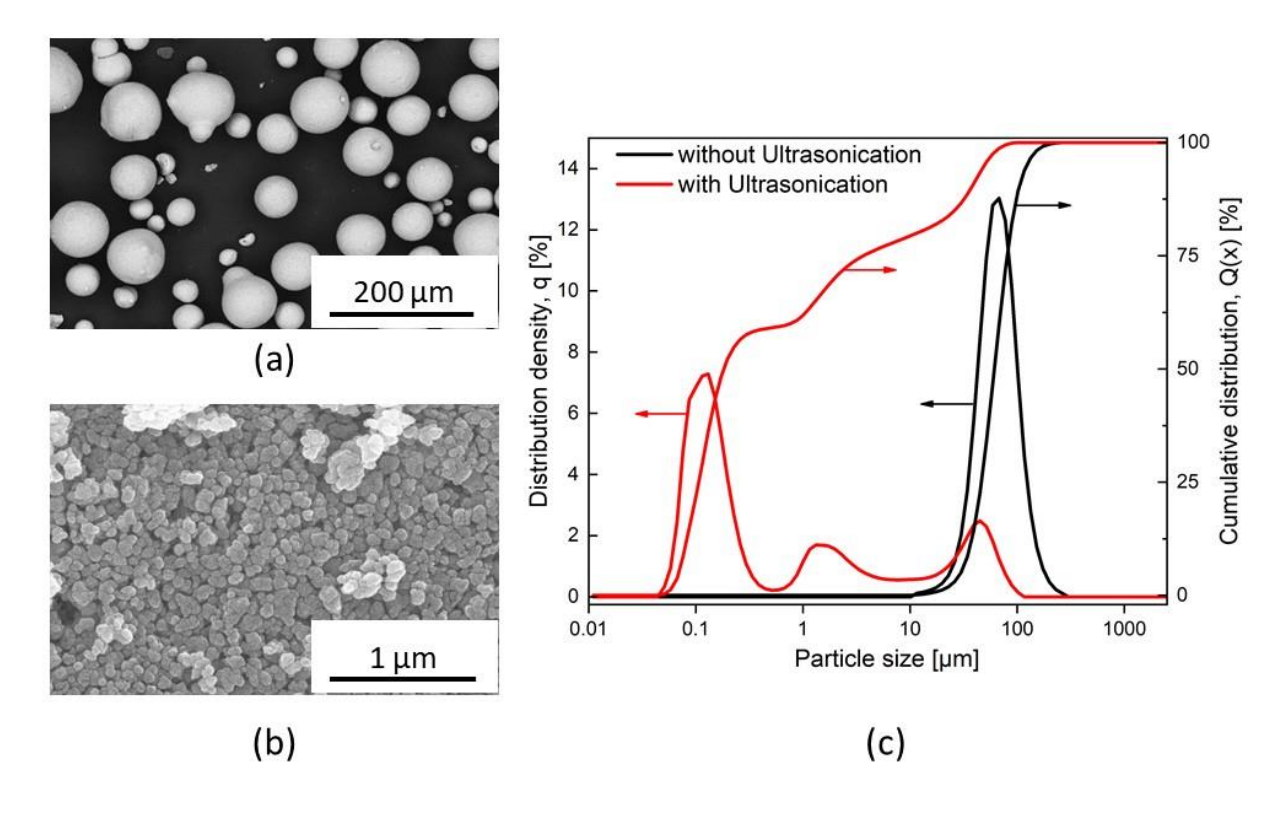


Fig. 3. Scanning electron micrographs of the 8YSZ powders: (a) as received condition, (b) after dispersing by ultra-sonification for 3 minutes and (c) particle size distributions.

The particle size distribution of the spray dried 8YSZ results correspond to $d_{10} = 35 \, \mu \text{m}$, $d_{50} = 61 \, \mu \text{m}$ and $d_{90} = 103 \, \mu \text{m}$, which suggests that the as-received particles are agglomerated. To investigate the primary particle size distributions, the powder was mixed with ethanol and the solvent dispersed with ultrasonic support for 3 minutes. The resulting particle size distribution is characterized by to $d_{10} = 0.078 \, \mu \text{m}$, $d_{50} = 0.172 \, \mu \text{m}$ and $d_{90} = 28 \, \mu \text{m}$. Nevertheless, it has also been observed that after the ultrasonic treatment the powder indicates a tri-modal distribution, which suggests that there are still some coarser particles (between 10-100 μm), which are strongly bonded with each other. The deposition process was carried out by utilizing the as-received spray dried 8YSZ powder, which were in the agglomerated state as shown in Fig. 3 (a).

3.2. Influence of AD process parameters

3.2.1. Effect of substrate materials and its preparation

Deposition of materials by AD is based on the impact of particles on the substrate or already deposited particles, where part of the kinetic energy is converted into bonding energy. In the initial

stage, the adhesion of the particles are suggested to be a result of the creation of an anchor layer related to mechanical entanglement (Ref 9). To understand the influence of the substrate material and its preparation on adhesion and homogeneity of the deposited coating on the substrate, 8YSZ particles were deposited by the AD process on three different substrate materials: stainless steel (grade 1.4571), copper and 3 wt% Mg-Al alloy. Where it should be noted that the hardness of the stainless steel is larger than the hardness of copper, which is larger than the hardness of AlMg₃ alloy. Furthermore, all the three substrates were prepared in two different conditions as mentioned in section 2.2. The substrates which were polished had a surface roughness (R_a) of 45-70 nm and the grit blasted (F-150) substrates a surface roughness (R_a) of 600-800 nm. The AD processing parameters for the deposition are summarised in Table 1.

Table 1: AD deposition parameters used for the samples shown in Figure 4 (a, b and c)

Stand-off	Traverse	No. of passes	Aerosol	Deposition	Total carrier
distance	speed		chamber	chamber	gas flow
(mm)	(mm/s)		pressure,	pressure	(slpm)
			feeder (mbar)	(mbar)	
10	30	30	(a) 615 (b) 610 (c) 558	(a) 1.1 (b) 1.0 (c) 1.2	15

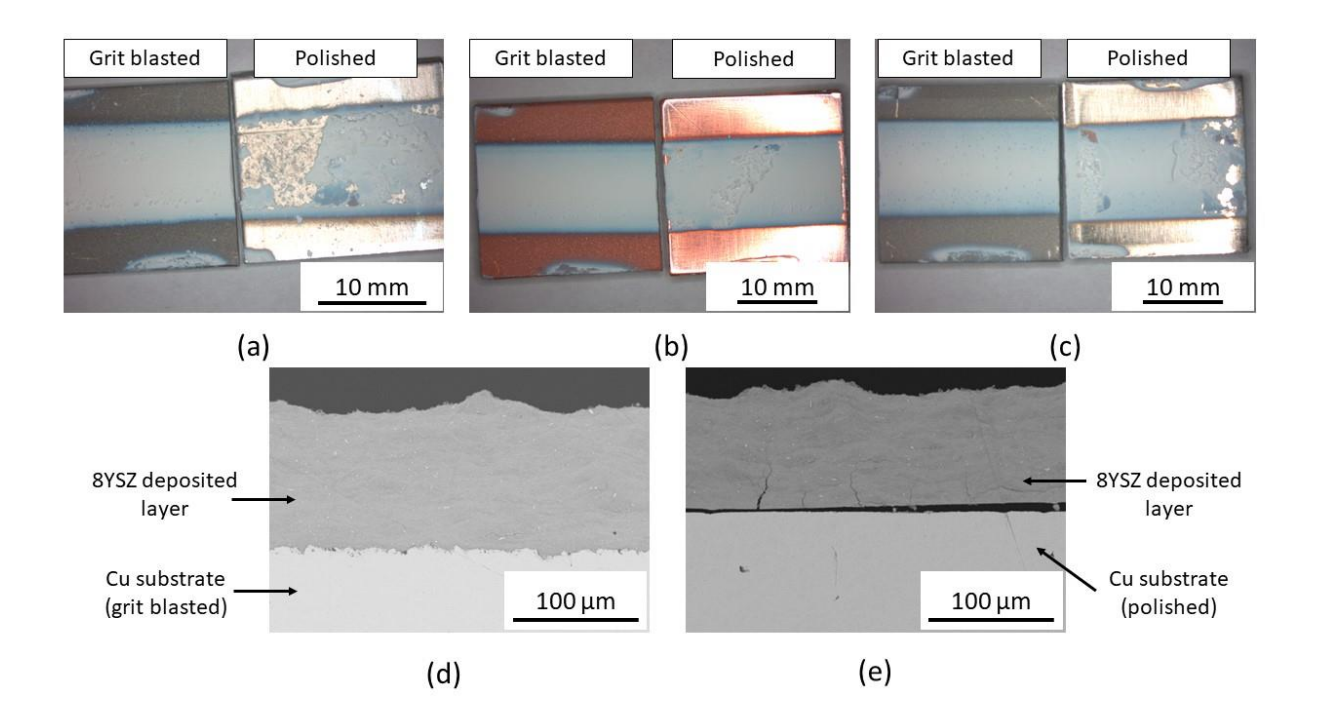


Fig. 4. Optical images illustrating the effect of substrate materials on deposited layers, (a) stainless steel (b) copper and (c) 3 wt% Mg-Al alloy substrate and SEM micrographs of cross-section showing the influence of the substrate surface roughness on the adhesion of the coating and the copper substrate, (d) grit blasted F150; (e) polished.

Figure 4 (a, b and c) shows optical microscopy images of the 8YSZ coatings on the three different substrates. It can be seen that, when the AD process parameters are the ones summarized in Table 1, an uniform and homogeneous layer was deposited on all three substrates, whose surfaces were prepared with grit blasting (F-150), whereas the polished substrates show a non-uniform coating, which tends to spall-off from the substrate. This indicates that the adhesion of 8YSZ coating on an as-received substrate is very poor. Furthermore, complementary SEM micrographs confirm the poor adhesion between the deposited layer and all three different substrates in comparison to substrates prepared by grit blasting. The dependency of the adhesion of the coatings on the substrate preparation is illustrated in SEM micrographs of the copper substrate in Fig. 4 (d & e). A very poor adhesion between the substrate and the deposited layers of 8YSZ on the polished substrate can be observed, while in the case of the copper substrate prepared by grit blasting (F150) a good adhesion between the substrate and the deposited 8YSZ layers was revealed.

This indicates that the initial substrate roughness is an important parameter in achieving a good deposition. In the current work, when the surface roughness was increased from 70 nm to 800 nm, the deposited layer not only exhibited a good adhesion but also a higher thickness. Further increase in the substrate roughness to 4200 nm by grit blasting yielded a very inhomogeneous deposition layer with completely uncoated regions of the substrate (these results are not included here in further detail). This finding suggests that a fine surface roughness in the range of primary particle size is required to achieve good adhesion between the substrate and the deposited film. Similar results have been reported in the literature. Kim et. al. (Ref 23) investigated the influence of the substrate roughness (Al₂O₃) on the deposition of Al₂O₃ film by the AD process. They observed an increment of the substrate roughness from 400 to 900 nm decreased the deposition rate, whereas for substrate roughness (R_a) above 1500 nm no deposition occurred. To summarize the current results, deposition rate and adhesion of the coatings depend on the initial substrate roughness, where a comparable substrate roughness to the starting materials' average particle size appears to be beneficial.

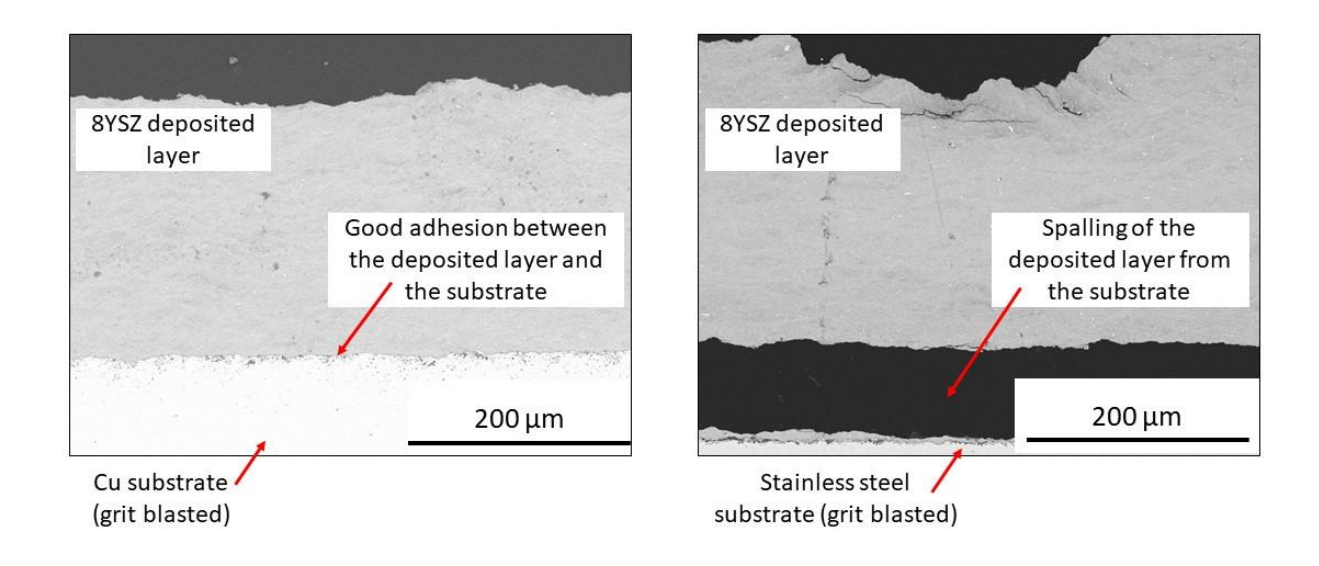


Fig. 5. SEM micrographs of the 8YSZ deposited layer by AD process at a carrier gas flow of 10 slpm on copper and stainless steel, showing good adhesion for the copper substrate and inferior interface quality for the stainless-steel substrate with the formation of cracks in the coating.

Further analysis with respect to the influence of the substrate materials on the coating properties indicates that the deposition efficiency on the stainless-steel substrate is low as compared to the deposition efficiency on the copper and 3wt% Mg–Al substrate. Furthermore, SEM micrographs of the deposited layer on the stainless-steel substrate show delamination close to the substrate and cracks parallel to the film surface were observed, which implies again that the substrate materials' hardness has an influence on the quality of interface and coating. This has been observed for different processing parameters and one example is shown in the SEM micrographs in Fig. 5. This suggests that the initial anchor layer formation at the interface was easier on a soft substrate material like, Cu and 3wt% Mg–Al. However, due to the high hardness of the stainless-steel substrate it may be difficult to form such an anchoring layer. Further investigation on the influence of the AD processing parameters on the deposition of 8YSZ was carried out for the copper substrate.

3.2.2. Effect of carrier gas flow

The flow of the carrier gas is directly influencing the particle velocity in the aerosol deposition process. According to the literature (Ref 7,24) the particle impact velocity is one of the most important processing parameters in the AD process. If at very low particle velocity not sufficient kinetic energy is provided for the successful deposition, the particles are bouncing back from the substrate. On the other hand, if the particle velocity is too high, abrasion of the substrate occurs. Hence, it was suggested that a successful deposition is only possible in a window of deposition with respect to the particle velocity (Ref 7).

In this section, the effect of the gas flows, which directly influence the particle velocity, is studied in case of the deposition of 8YSZ on the copper substrate. All the other processing parameters e.g., stand-off distance, traverse speed, deposition chamber pressure etc. are kept constant while only the total carrier gas flow is varied, i.e. (i) 5 slpm, (ii) 10 slpm, (iii) 15 slpm, (iv) 20 slpm, (v) 25 slpm, (vi) 30 slpm. All the other AD process parameters are summarized in Table 2.

Table 2: AD deposition parameters for the samples shown in Fig. 6

Stand-off distance	Traverse speed	No. of passes	Deposition chamber
(mm)	(mm/s)		pressure (mbar)
10	30	30	1

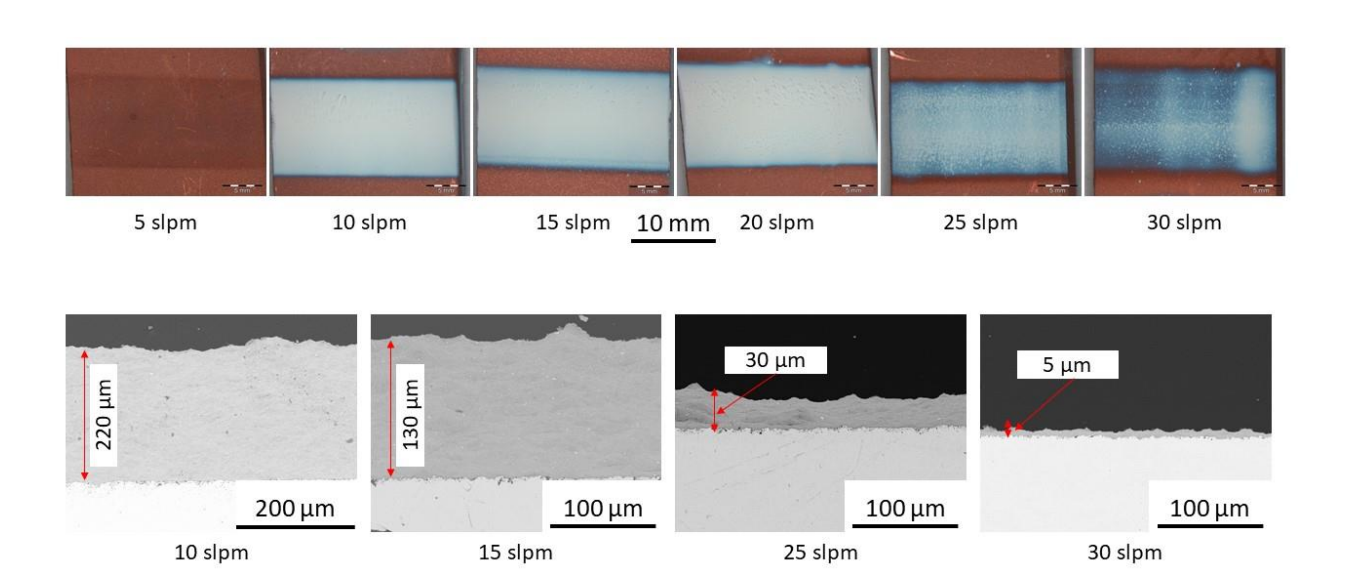


Fig. 6. Top: Optical images of the specimens showing the deposited 8YSZ layer on the copper substrates at varied carrier gas flows. Bottom: SEM micrographs of the deposited 8YSZ layers at four different flows.

The top set of images in Fig. 6 shows the optical images of the 8YSZ deposited layers deposited by AD process on copper substrate materials at varied carrier gas flows. The optical images suggest that above a carrier gas flow of 5 slpm the deposition of the 8YSZ materials on the both substrates occurred. However, the deposited layer thickness is lower at a carrier gas flow above 20 slpm. The bottom set of the images in Fig. 6 shows the SEM micrographs of the deposited layers. The interface quality between the coating and the substrate for all the different flows are good. The deposition at a very small carrier gas flow, i.e. 5 slpm, did not result in any deposition. The deposition at a carrier gas flows of 15 slpm shows the highest deposition rate among all the used carrier gas flows. However, carrier gas flow of higher than 15 slpm the deposition rate reduces with increasing carrier gas flow.

In the current work, a window regarding deposition in case of the AD process is also observed, where it can be seen that when the carrier gas flow is 5 slpm the deposition does not occur, as verified in Figure 6. When the carrier gas flow is increased to 10 slpm and above the deposition of 8YSZ occurs. Furthermore, it can be observed that with the flows of 25 slpm and 30 slpm, the coating thickness is very thinner as compared to the coatings deposited with flows of 10 slpm and 20 slpm. This indicates that in the case of coatings deposited with flows of 25 slpm onwards, the particle velocities might be very close to the erosion velocity (V_E , AD). It is possible that with these high velocities powders particles only create craters in the substrate at the begin of the deposition process. After performing few scans of deposition on the surface a very thin coating develops and forthcoming particles which come in contact with the already deposited layers tend to be deflected. However, such erosion of the substrate could not be clearly verified in the current work.

3.2.3. Influence of the carrier gas species

The particle velocity has a strong influence on the deposition rate and the coating properties in the AD process. In fact, the particle velocity can also be influenced by changing the carrier gas species. It is possible to improve the particle acceleration and impact velocity by using helium (due to the low molar mass of helium) as a carrier gas. To study the influence of the carrier gas species six different AD experiments were carried out, where helium and argon have been used as the carrier gas. Three different carrier gas flows, 5, 10 and 15 slpm were used in this set of experiments. The deposition of the 8YSZ powder has been performed on copper substrates, which were grit blasted (F-150) prior to the deposition. The AD processing parameters for the samples shown in Figure 7 are as summarized in Table 3, where the carrier gas flow were 5, 10 and 15 slpm.

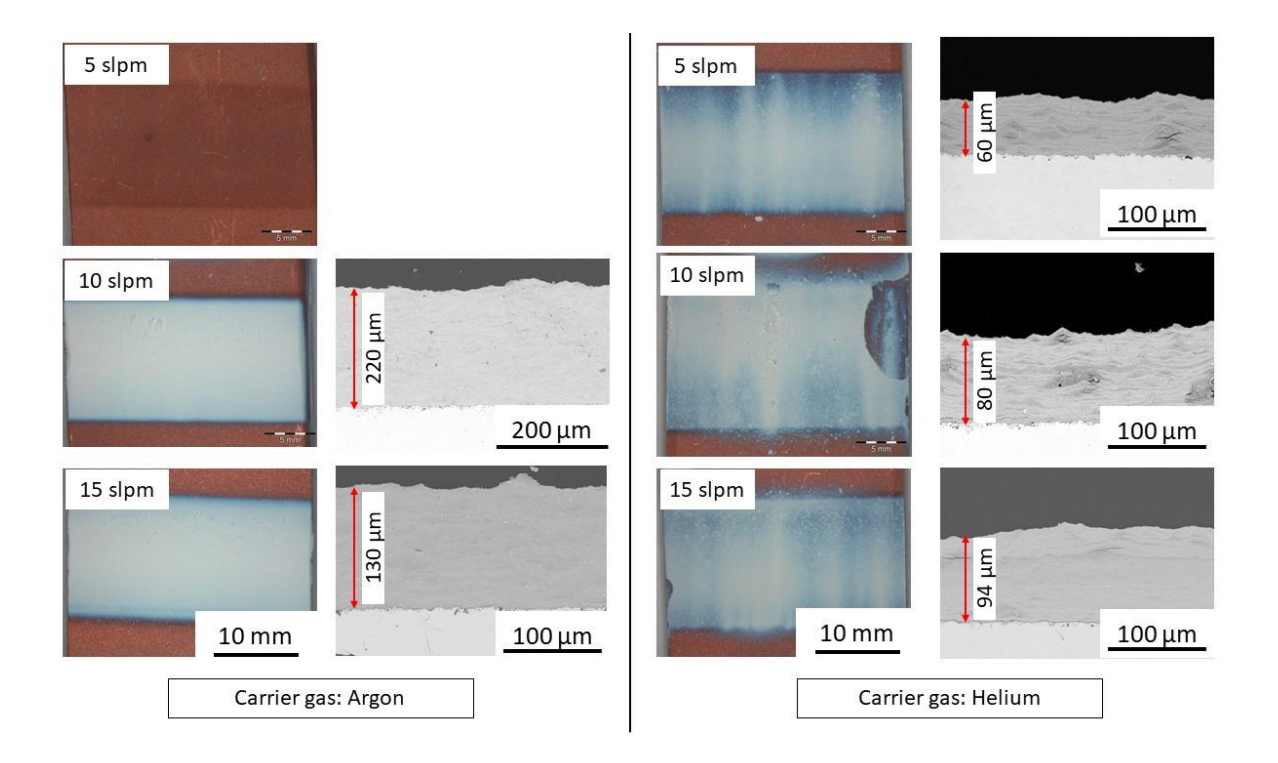


Fig. 7. Optical images of 8YSZ coatings after deposition and the SEM micrographs of the respective specimens; left side images- argon as carrier gas; Right side images- helium as carrier gas; with variation of carrier gas flows (a) 5 slpm, (b) 10 slpm, (c) 15 slpm.

From the optical images shown in Figure 7, it can be observed that at a low carrier gas flow (5 slpm) deposition of 8YSZ is possible using Helium unlike in the case of argon as a carrier gas. Nevertheless, for the carrier gas flow rates 10 and 15 slpm, the deposition efficiency was higher when argon was used as a carrier gas. Furthermore, the microstructure of the deposited layers by helium as carrier gas revealed cracks parallel to the film surface. When helium was used as a carrier gas the coatings were delaminated, the coatings show a better adhesion to the substrate in case of argon as a carrier gas. However, SEM micrographs indicate that although the adhesion between substrate and coating layer was good the inter-particle bonding was weak in case of helium being the carrier gas, resulting in an irregular and porous coating. These results indicate that it might be possible that the submicron sized 8YSZ particles achieve a very high velocity using helium as a carrier gas, being close to the erosion velocity and hence, reducing the deposition efficiency.

3.2.4. Modelling and simulation of carrier gas velocity

In this work, the deposition efficiency that is the ratio between the mass of powder consumed from the aerosol chamber and the mass of the powder deposited on the substrate of the AD process was below 2%. This suggest that not all the particles transported to the deposition chamber were deposited on the substrate. Lee et al. (Ref 25) used computational fluid dynamic simulation to study the effect of nozzle geometry on the coating quality by AD process. They reported optimization of the nozzle geometry is important to reduce the shockwaves in the gas flow between the nozzle and the substrate, which, leads to poor coating quality. Similarly, Johnson et al. (Ref 26) also reported that among different AD process parameters, optimization of the nozzle geometry is necessary for improving the deposition efficiency of the AD process.

The gas flow for the nozzle used in this work was simulated for a carrier gas flow rate of 10 splm and a chamber pressure of 1 mbar for two cases: without presence of a substrate and with a substrate (at a distance of 10 mm from the nozzle). Fig. 8 shows results of simulation of the gas flow with and without presence of a substrate. The colour bar indicates the gas velocity attains during the AD process. The simulation results show that the gas attains a high velocity of about 540 m/s (approx. mach 10) upon exiting the nozzle into the deposition chamber. Since the pressure directly at the nozzle throat is still much higher (approx. 50 mbar) than the pressure of the deposition chamber (1 mbar), a very strong gas expansion was observed. This was in particular pronounced in the direction perpendicular to the slit plane of the nozzle (Fig. 8 (b)) which is not desired.

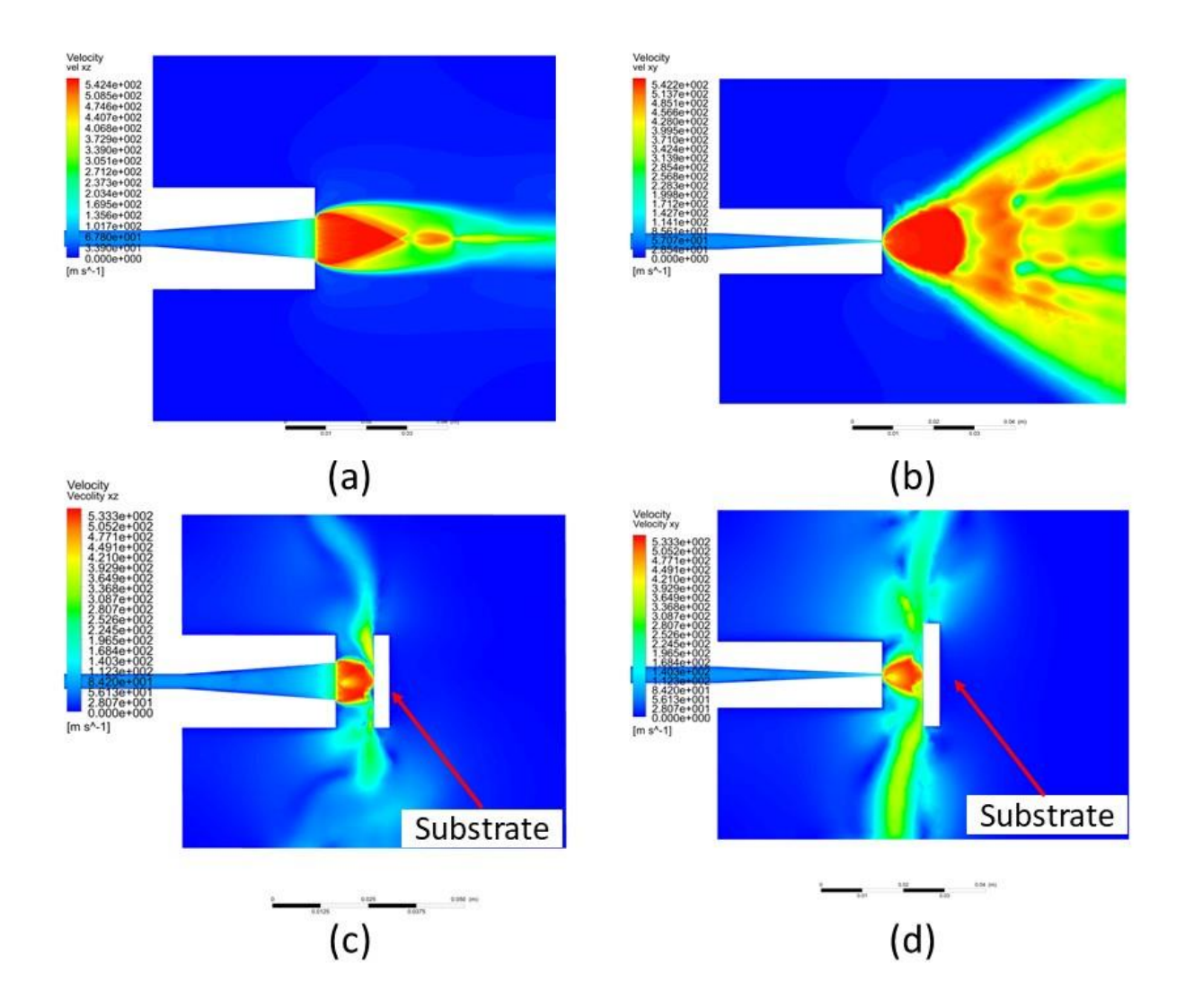


Fig. 8. CFD simulation result of the carrier gas velocity without substrate (a) XZ direction (parallel to the nozzle movement direction), (b) XY direction (transverse to the nozzle movement direction (a and b) and with substrate (c) XZ direction (parallel to the nozzle movement direction), (d) XY direction (transverse to the nozzle movement direction.

Furthermore, the expansion of the gas accompanied by a shock wave as can be seen in Fig. 8 (b). When the nozzle configuration deviates from correctly expanded gas flow, it generates an undesirable shear layer, and a reflected compression shock, which decrease the kinetic energy of the gas flow and in turn particle flow which adversely affects the overall coating quality (Ref 25). The nozzle used in this work therefore still needs to be optimized as shockwave-induced fluctuations can yield non-uniform coating and lower the deposition efficiency.

3.2.4. Characterization of the 8YSZ deposited layer

In the current work a suitable AD processing parameter set was selected for further characterization of the coating. For detailed characterizations of deposited coatings, in total three specimens, deposited by different carrier gas flows (10 slpm, 15 slpm and 20 slpm), were selected. The 8YSZ powder was deposited by AD process on copper substrates with a traverse speed of 30 mm/s and a total number of scans of 30. The substrates were grit blasted (F-150) prior to the deposition process and argon was used as the carrier gas.

Fig. 9 shows the X-ray diffraction (XRD) patterns of 8YSZ starting powder (black line) and the AD process deposited 8YSZ layer (top surface) at a carrier gas flow of 10 slpm and argon as the carrier gas for the sample shown in Fig. 7. There is no significant difference in the diffractograms of the powder and the deposited coating. This confirms that the cubic phases of feedstock 8YSZ powder is retained in the deposited coating. Moreover, from the calculation of the full width of half maximum (FWHM), there is no significant broadening of the diffracted peaks. The domain size (~ 27–29 nm) and the lattice constant remains constant for the feedstock-powder and the deposited coating. The reason for not obtaining significant broadening of the XRD peak might be related to the fact that the XRD measurement was conducted on the surface of the coating (Ref 27). The surface layer of the coating appears to be rather non-deformed, compared to layer close to the substrate, since this was the last layer during the deposition process. The layer close to the substrate was deformed by the oncoming particles. This will be discussed later in this manuscript regarding effects on the mechanical properties. One of the advantages of the AD process is that, due to the room temperature deposition, it is possible to retain the original phase of the starting material in the deposited layer. This is confirmed by the current work, where the 8YSZ retains its original cubic phase after deposition, as verified in Fig. 9.

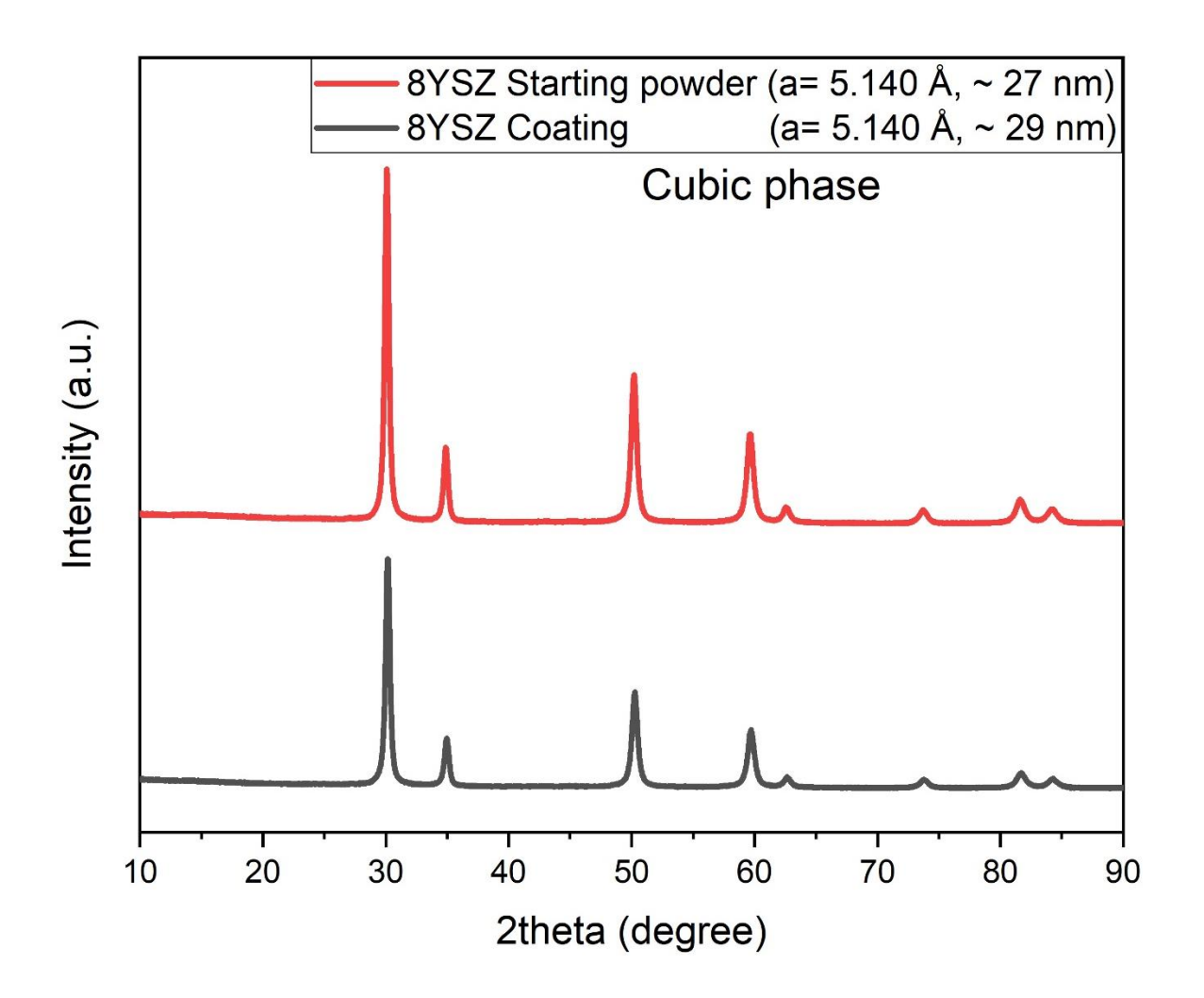


Fig. 9 XRD patterns of 8YSZ powder (red) and by AD deposited 8YSZ layer on copper substrate (black).

Fig. 10 illustrates the surface topography of the AD process deposited 8YSZ layers for three different carrier gas flows. The deposited coatings' surfaces show a wave like structure in x-direction (parallel to the nozzle movement direction). The coatings have a larger thickness at the centre compare to the edge in y-direction (transverse to the nozzle movement direction). The arithmetic mean surface roughness of the coatings varies between $R_a = 3 - 5 \mu m$, however, for thicker coatings (500 μ m) the roughness increases to $R_a \sim 11 \mu m$.

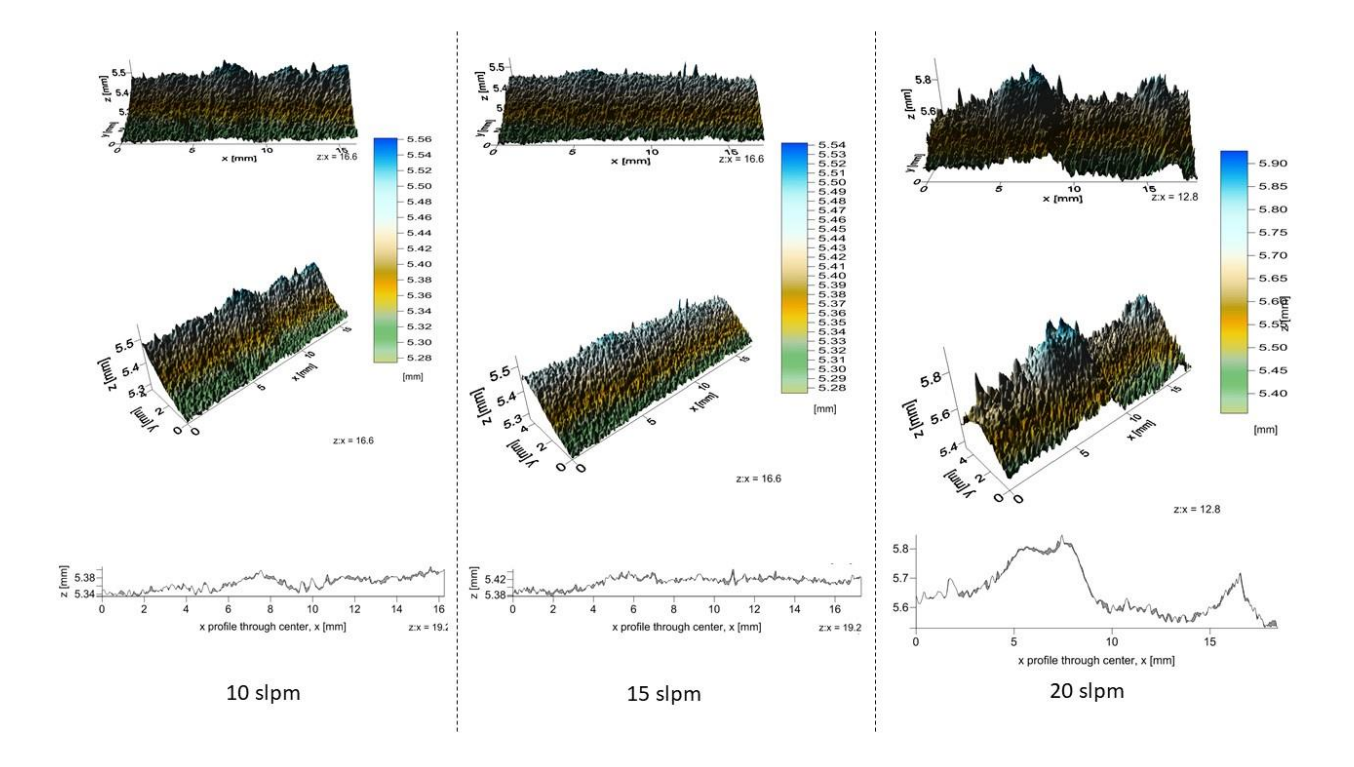


Fig. 10 Surface morphology of 8YSZ coating with flow of (a) 10 slpm (b) 15 slpm (c) 20 slpm and the stand-off distance of 10 mm showing a wave like surface in x-direction (top images). The middle images showing the topography in y-direction and the bottom image, showing the variation of R_a values in x-direction.

The hardness (*H*) of the coatings was studied at different positions with respect to the substrate coating interface. The deposited layer at a carrier gas flow rate of 10 slpm yielded higher hardness values than the layers deposited at carrier gas flow rates of 15 and 20 slpm. Striking feature of the hardness measurement is a gradient of the hardness values across the thickness in the coatings deposited at three different carrier gas flow. Higher hardness values are obtained near the interface and lower values further away from the interface (near the top surface of the layer) for all the three specimens. The average hardness results (from 20 indentations) for the 8YSZ deposited layer at three different carrier gas flow, i.e. 10, 15 and 20 slpm are shown in Fig. 11 (a). The gradient in the hardness of the coating which was deposited at a carrier gas flow of 10 slpm with respect to the position from the interface is presented in Fig. 11 (b) and an optical image of the indentation imprints for the same coating is shown in Fig. 11 (c).

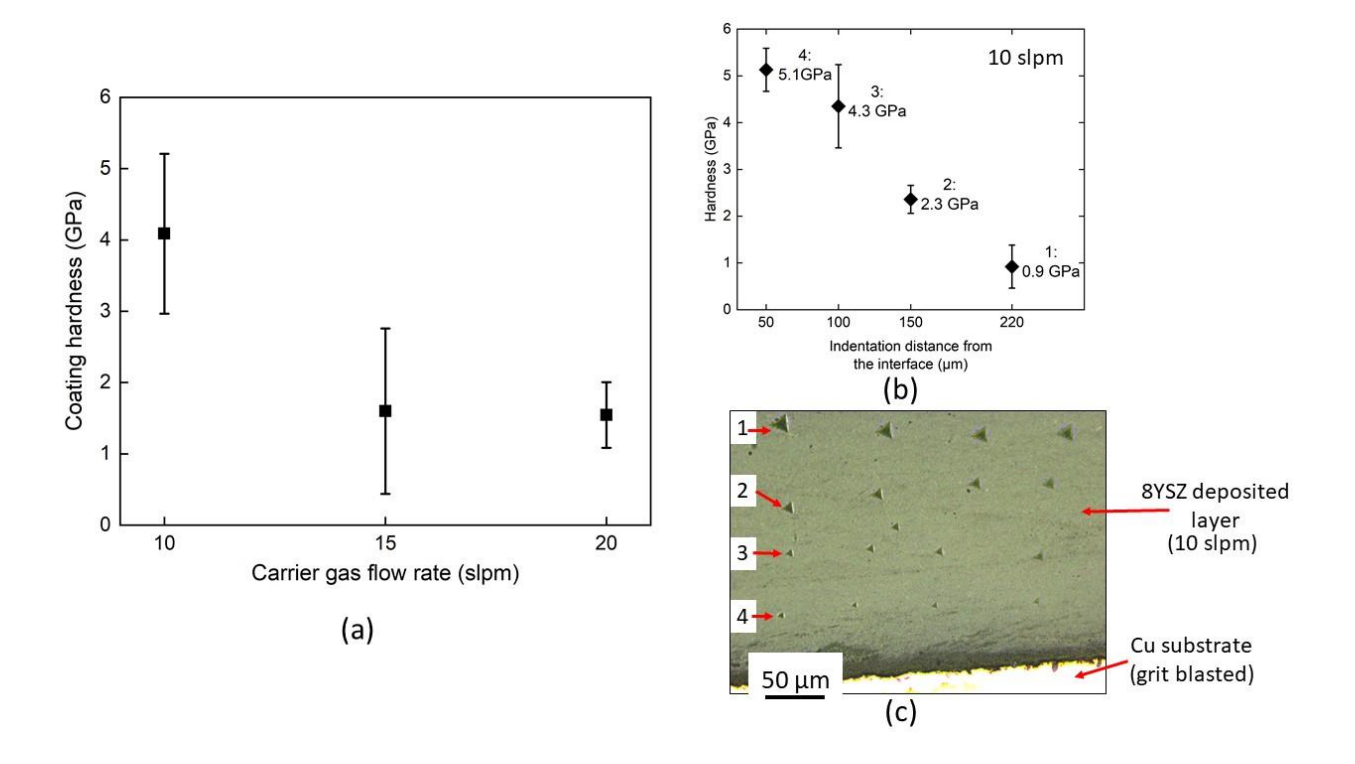


Fig. 11. Average hardness (*H*) of the 8YSZ deposited layer for different carrier gas flow rates, (b) Hardness (*H*) of the 8YSZ deposited layer (carrier gas flow: 10 slpm) at different position from the interface showing the gradient in the hardness values and (c) Optical images of the indentation imprints (load 10 mN) in the deposited layer (carrier gas flow: 10 slpm)

These results confirm the importance of the hammering effect for the deposited layer. Fundamental studies on the understanding of the mechanism of the aerosol deposition process usually suggest that the high kinetic energy and strain rate lead to fracturing of the primary particles upon collision with the substrate. Furthermore, continuous bombardment of the particles on the deposited layer, so-called hammering effect is responsible for further deformation and consolidation of the layers (Ref 6,7,23,27).

Taking a closer look at the results it appears that there is a relationship between the average hardness and the thickness of the particular coating. The thickness of the deposited layer at a carrier gas flow rate of 10 slpm is approximately 220 μ m, where the coating thickness of the specimen deposited at a carrier gas flow rate of 15 and 20 slpm is approximately 100 μ m, as illustrated in Fig. 6. The high average hardness value of the deposited layer at a carrier gas flow rate of 10 slpm

can be explained by higher hammering effect as more material has been deposited on the substrate as compared to the specimen where the carrier gas flow rate is 15 and 20 slpm. While kinetic energy is an important parameter for the deposition to take place, it is certainly not the only influence factor, since in case of very high velocities (where the carrier gas flow rate was higher i.e., 15 and 20 slpm) the mechanical properties are lower than in case of the coating which was obtained at a lower carrier gas flow rate (i.e. 10 slpm). Looking at the absolute values, it is also obvious that the measured hardness values of the AD coatings are much lower than those reported for bulk YSZ materials (Ref 28), which indicates that the layers still contain a large amount of fine pores.

The average porosity was measured by digital image analysis (software used: Image J) on the basis of the high resolution SEM micrographs of cross-sections of the specimens (Ref 29). An example of such a SEM micrograph for a carrier gas flow of 10 slpm is presented in Fig. 12 (a & b). The porosity measurement by digital image analysis shows that the volume fraction of porosity present in the coating, which was deposited at a carrier gas flow of 10 slpm was approximately 45.6%. Additionally to the digital image analysis, mercury intrusion porosimetry (MIP) technique was used to further characterize the pore volume of the coating on a different specimen (sample b), which was also deposited at a carrier gas flow of 10 slpm. The MIP result confirms the presence of high volumetric porosity of approximately 55% in the AD coating however, 91% of the pore size lies between 10 nm to 100 nm, as shown in Fig. 12 (c).

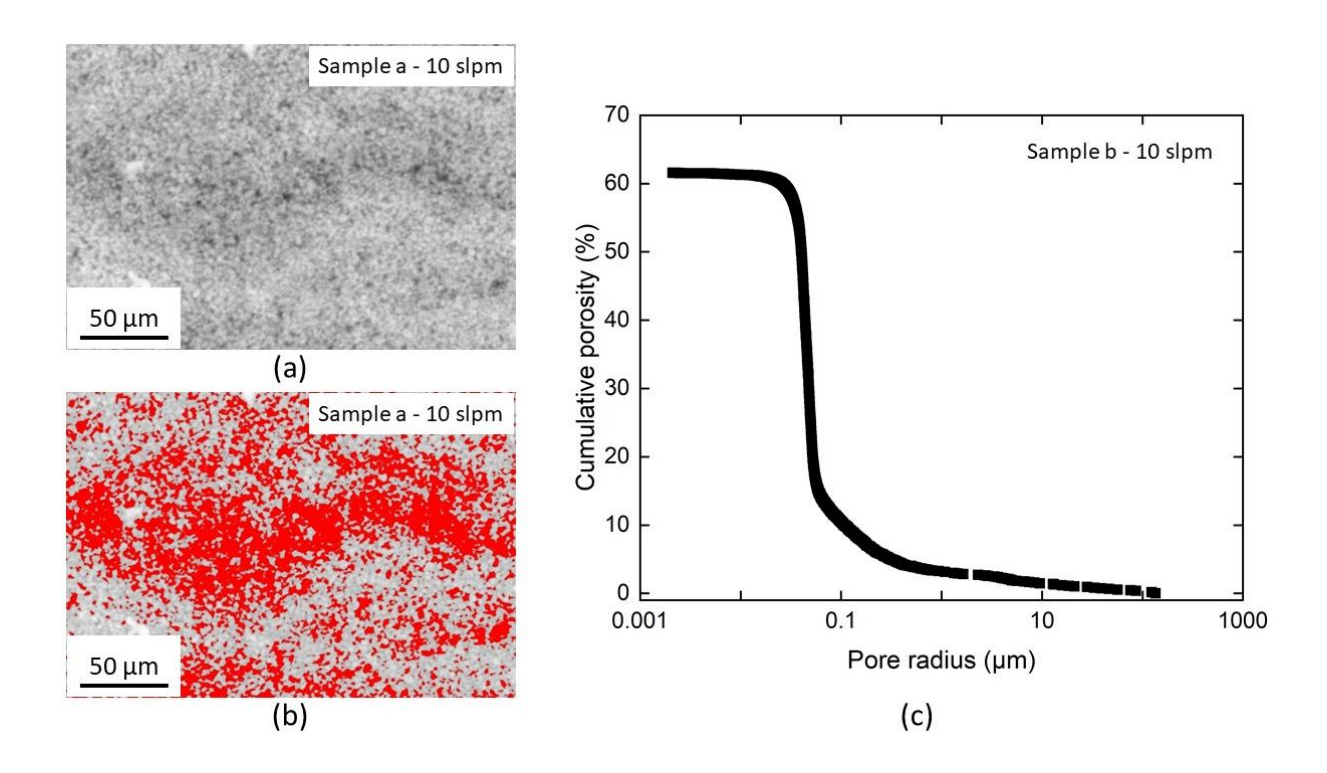


Fig. 12 (a) High resolution SEM micrograph of 8YSZ coating deposited on a Cu substrate by AD at a carrier gas flow of 10 slpm (b) colour threshold for porosity calculation and (c) pore size distribution of a different 8YSZ coating on a Cu substrate by AD at a carrier gas flow of 10 slpm obtained by Hg intrusion.

4. Conclusion

8mol% Yttrium Stabilized Zirconia (8YSZ) is successfully deposited by an aerosol deposition process at room temperature. The use of a dispersion nozzle between the aerosol chamber and the deposition chamber verified to be successful to de-agglomerate the aerosolized particles prior to deposition, hence, improving coatings quality and homogeneity. Influence of various AD processing parameters on the properties of coating and interface quality has been studied. The substrate material affected the interface quality and the inter-layer bonding of the AD deposited layer, where the adhesion between coating and stainless-steel substrate revealed poor interface quality and inhomogeneous layers as compared to deposition on copper and AlMg₃. The difference in the coating properties can be attributed to the hardness of the substrate, where a low hardness substrate appears to be more favourable for the AD deposition process. Additionally, an intermediate surface roughness of the substrate is advantageous for a better adhesion between

coating and substrate. A deposition window is suggested to be present in the case of the aerosol deposition process, where a successful deposition only occurs above a critical velocity, which could be achieved carrier gas flows above 5 slpm. However, at a higher carrier gas flow (i.e., 25 slpm) the deposition rate significantly decreased. Nevertheless, the deposition efficiency for all the different processing parameters was below 2%.

The hardness measurement of the coatings at different positions from the interface showed a gradient in the hardness, where the hardness values decrease with increasing distance from the interface. The particles deposited first are continuously compacted during deposition of particles on top. This remarkable result contributes to the proposed mechanism, where the deposition and growth of the coating occurs in association with a hammering effect that deforms and consolidates the primary particle. Nevertheless, the absolute values of the hardness of these AD coatings are much lower than those of dense bulk 8YSZ material. Further analysis of the porosity of the coatings by digital image analysis and mercury porosimetry revealed that the layers still contain a large amount of fine pores.

The result demonstrated the feasibility of applying an aerosol deposition method for fabricating different electrochemical materials, where interparticle diffusion is a challenge due to typically necessary high processing temperatures.

Acknowledgements

The authors would like to express our thanks to Mr. Karl-Heinz Rauwald, for his technical assistance on developing the Aerosol Deposition facility.

References

- 1. F. Shi, "Ceramic Coatings: Applications in Engineering," BoD Books on Demand, 2012.
- 2. V. Matikainen, K. Niemi, H. Koivuluoto, and P. Vuoristo, Abrasion, Erosion and Cavitation Erosion Wear Properties of Thermally Sprayed Alumina Based Coatings, *Coatings*, Multidisciplinary Digital Publishing Institute, 2014, **4**(1), p 18–36.
- 3. "Beyond Traditional Coatings: A Review on Thermal-Sprayed Functional and Smart Coatings | SpringerLink," n.d., https://link.springer.com/article/10.1007/s11666-019-00857-1. Accessed 27 March 2020.
- 4. M.N. Rahaman, "Sintering of Ceramics," CRC Press, 2007.

- 5. J. Akedo and M. Lebedev, Microstructure and Electrical Properties of Lead Zirconate Titanate (Pb(Zr52/Ti48)O3) Thick Films Deposited by Aerosol Deposition Method, *Jpn. J. Appl. Phys.*, IOP Publishing, 1999, **38**(9S), p 5397.
- 6. J. Akedo, Room Temperature Impact Consolidation (RTIC) of Fine Ceramic Powder by Aerosol Deposition Method and Applications to Microdevices, *J Therm Spray Tech*, 2008, **17**(2), p 181–198.
- 7. "Hanft: An Overview of the Aerosol Deposition Method:... Google Scholar," n.d., https://scholar.google.com/scholar_lookup?title=An%20overview%20of%20the%20aerosol%20deposition%20method%3A%20Process%20fundamentals%20and%20new%20trends%20in%20materials%20applications&journal=J.%20Ceram.%20Sci.%20Technol&volume=6&pages=147-182&publication_year=2015&author=Hanft%2CD. Accessed 27 March 2020.
- 8. J. Akedo, Room Temperature Impact Consolidation and Application to Ceramic Coatings: Aerosol Deposition Method, *Journal of the Ceramic Society of Japan*, 2020, **128**(3), p 101–116.
- 9. D.-W. Lee, H.-J. Kim, Y.-H. Kim, Y.-H. Yun, and S.-M. Nam, Growth Process of α-Al2O3 Ceramic Films on Metal Substrates Fabricated at Room Temperature by Aerosol Deposition, *Journal of the American Ceramic Society*, 2011, **94**(9), p 3131–3138.
- 10. J.-G. Liang, C. Wang, Z. Yao, M.-Q. Liu, H.-K. Kim, J.-M. Oh, and N.-Y. Kim, Preparation of Ultrasensitive Humidity-Sensing Films by Aerosol Deposition, *ACS Appl. Mater. Interfaces*, American Chemical Society, 2018, **10**(1), p 851–863.
- 11. C. Lee, M.-Y. Cho, M. Kim, J. Jang, Y. Oh, K. Oh, S. Kim, B. Park, B. Kim, S.-M. Koo, J.-M. Oh, and D. Lee, Applicability of Aerosol Deposition Process for Flexible Electronic Device and Determining the Film Formation Mechanism with Cushioning Effects, *Scientific Reports*, Nature Publishing Group, 2019, **9**(1), p 1–10.
- 12. F. Han, R. Mücke, T. Van Gestel, A. Leonide, N.H. Menzler, H.P. Buchkremer, and D. Stöver, Novel High-Performance Solid Oxide Fuel Cells with Bulk Ionic Conductance Dominated Thin-Film Electrolytes, *Journal of Power Sources*, 2012, **218**, p 157–162.
- 13. S. Suganuma, M. Watanabe, T. Kobayashi, and S. Wakabayashi, SO2 Gas Sensor Utilizing Stabilized Zirconia and Sulfate Salts with a New Working Mechanism, *Solid State Ionics*, 1999, **126**(1), p 175–179.
- 14. R. Vassen, A. Stuke, and D. Stöver, Recent Developments in the Field of Thermal Barrier Coatings, *J Therm Spray Tech*, 2009, **18**(2), p 181–186.
- 15. L.B. Chen, Yttria-Stabilized Zirconia Thermal Barrier Coatings a Review, *Surf. Rev. Lett.*, World Scientific Publishing Co., 2006, **13**(05), p 535–544.
- 16. G. Montavon, RECENT DEVELOPMENTS IN THERMAL SPRAYING FOR IMPROVED COATING CHARACTERISTICS AND NEW APPLICATIONS/ PROCESS CONTROLS AND SPRAY PROCESSES, *HTM*, Begel House Inc., 2004, **8**(1), doi:10.1615/HighTempMatProc.v8.i1.50.
- 17. J.-J. Choi, J.-H. Choi, J. Ryu, B.-D. Hahn, J.-W. Kim, C.-W. Ahn, W.-H. Yoon, and D.-S. Park, Microstructural Evolution of YSZ Electrolyte Aerosol-Deposited on Porous NiO-YSZ, *Journal of the European Ceramic Society*, 2012, **32**(12), p 3249–3254.

- 18. J. Exner, G. Albrecht, D. Schönauer-Kamin, J. Kita, and R. Moos, Pulsed Polarization-Based NOx Sensors of YSZ Films Produced by the Aerosol Deposition Method and by Screen-Printing, *Sensors*, Multidisciplinary Digital Publishing Institute, 2017, **17**(8), p 1715.
- 19. E. Fuchita, E. Tokizaki, E. Ozawa, and Y. Sakka, Formation of Zirconia Films by Aerosol Gas Deposition Method Using Zirconia Powder Produced by Break-down Method, *Journal of the Ceramic Society of Japan*, 2010, **118**(1382), p 948–951.
- 20. G. Mauer and R. Vaßen, Plasma Spray-PVD: Plasma Characteristics and Impact on Coating Properties, *J. Phys.: Conf. Ser.*, 2012, **406**, p 012005.
- 21. C.T. Rueden, J. Schindelin, M.C. Hiner, B.E. DeZonia, A.E. Walter, E.T. Arena, and K.W. Eliceiri, ImageJ2: ImageJ for the next Generation of Scientific Image Data, *BMC Bioinformatics*, 2017, **18**(1), p 529.
- 22. "An Improved Technique for Determining Hardness and Elastic Modulus Using Load and Displacement Sensing Indentation Experiments | Journal of Materials Research | Cambridge Core," n.d., https://www.cambridge.org/core/journals/journal-of-materials-research/article/an-improved-technique-for-determining-hardness-and-elastic-modulus-using-load-and-displacement-sensing-indentation-experiments/A53D45298E14F73B86495BBC056E16DC. Accessed 1 April 2020.
- 23. C.-W. Kim, J.-H. Choi, H.-J. Kim, D.-W. Lee, C.-Y. Hyun, and S.-M. Nam, Effects of Interlayer Roughness on Deposition Rate and Morphology of Aerosol-Deposited Al2O3 Thick Films, *Ceramics International*, 2012, **38**(7), p 5621–5627.
- 24. "Aerosol Deposition of Ceramic Thick Films at Room Temperature: Densification Mechanism of Ceramic Layers Akedo 2006 Journal of the American Ceramic Society Wiley Online Library," n.d., https://ceramics.onlinelibrary.wiley.com/doi/full/10.1111/j.1551-2916.2006.01030.x. Accessed 27 March 2020.
- 25. M.W. Lee, J.J. Park, D.Y. Kim, S.S. Yoon, H.Y. Kim, D.H. Kim, S.C. James, S. Chandra, T. Coyle, J.H. Ryu, W.H. Yoon, and D.S. Park, Optimization of Supersonic Nozzle Flow for Titanium Dioxide Thin-Film Coating by Aerosol Deposition, *Journal of Aerosol Science*, 2011, **42**(11), p 771–780.
- 26. S.D. Johnson, D. Schwer, D.-S. Park, Y.-S. Park, and E.P. Gorzkowski, Deposition Efficiency of Barium Hexaferrite by Aerosol Deposition, *Surface and Coatings Technology*, 2017, **332**, p 542–549.
- 27. D.-W. Lee, O.-Y. Kwon, W.-J. Cho, J.-K. Song, and Y.-N. Kim, Characteristics and Mechanism of Cu Films Fabricated at Room Temperature by Aerosol Deposition, *Nanoscale Research Letters*, 2016, **11**(1), p 162.
- 28. L. Donzel and S.G. Roberts, Microstructure and Mechanical Properties of Cubic Zirconia (8YSZ)/SiC Nanocomposites, *Journal of the European Ceramic Society*, 2000, **20**(14), p 2457–2462.
- 29. H. Du, J.H. Shin, and S.W. Lee, Study on Porosity of Plasma-Sprayed Coatings by Digital Image Analysis Method, *Journal of Thermal Spray Technology*, 2005, **14**(4), p 453–461.